NASA Technical Memorandum 107582

RESULTS FOR THE HYBRID LAMINAR FLOW CONTROL EXPERIMENT CONDUCTED IN THE NASA LANGLEY 8-FT TRANSONIC PRESSURE TUNNEL ON A 7-FT CHORD MODEL

PERCY J. BOBBITT, JAMES C. FERRIS
WILLIAM D. HARVEY AND SURESH H. GORADIA

MARCH 1992

NASA
National Aeronautics and Space Administration
Langley Research Center
Hampton, Virginia 23665-5225

RESULTS FOR THE HYBRID LAMINAR FLOW CONTROL EXPERIMENT CONDUCTED IN THE NASA LANGLEY 8-FT TRANSONIC PRESSURE TUNNEL ON A 7-FT CHORD MODEL

Percy J. Bobbitt
Institute for Computer Applications in Science and Engineering
NASA Langley Research Center
Hampton, VA 23665

James C. Ferris and Wiliam D. Harvey
NASA Langley Research Center
Hampton, VA 23665

Suresh H. Goradia
Vigyan Inc.
Hampton, VA 23665

Abstract

A description is given of the developoment of, and results from, the hybrid laminar flow control (HLFC) experiment conducted in the NASA Langley 8-ft Transonic Pressure Tunnel on a 7-ft chord, 23° swept model. The methods/codes used to obtain the contours of the HLFC model surface and to define the suction requirements are outlined followed by a discussion of the model construction, suction system, instrumentation and some example results from the wind tunnel tests. Included in the latter are the effects of Mach number, Reynolds number, suction level and the extent of suction. The data show that, at or near the design Mach number ($M_\infty \approx 0.81$), large extents of laminar flow can be achieved with suction mass flows over the first 25%, or less, of the chord. Top surface drag coefficients with suction extending from near the leading edge to 20% of the chord were approximately 40% lower than those obtained with no suction. The results indicate that HLFC can be designed for transonic speeds with lift and drag coefficients approaching those of LFC designs.

I. Introduction

A number of drag reduction research projects were undertaken in the mid 1970's as part of NASA's Aircraft Energy Efficient (ACEE) Progam[1]. Some were expedited within NASA and others by industry. Included in the former were two experiments carried out in the Langley Research Center's 8-ft Transonic Pressure Tunnel (8-ft TPT) pertaining to laminar flow control (LFC). Both were performed with a 23 degree swept airfoil model of 7 foot chord which spanned the tunnel from floor to ceiling. A streamline liner was installed on the walls of the contraction and test section to provide flow about the model equivalent to that about an infinite-span, yawed wing.

The first of the two LFC experiments conducted was instigated by Dr. W. Pfenninger and employed both slotted and perforated surfaces (not at the same time) on the upper surface of the model[2-12]. The second LFC experiment, which is the subject of the present paper, employed a perforated suction surface over the first 25% of the top side of the airfoil and a solid surface over the remaining 75%. An airfoil or wing with partial chord suction such as this is usually referred to as a hybrid laminar flow control (HLFC) concept. Laminar flow is maintained initially by surface suction (an adverse pressure gradient may also be used) while downstream of the region of suction laminar flow is maintained by a favorable pressure gradient. A slotted suction surface was utilized on the lower or bottom side of the airfoil model for both experiments.

Testing of the LFC airfoil with slotted upper and lower surfaces began in the spring of 1981 but a number of substantial hardware problems delayed serious research testing until late in 1983. The slotted LFC tests were completed in the spring of 1985 and the model dismantled and reassembled with a perforated upper surface in the late summer of 1985. These tests were completed in the fall of 1987 and the HLFC test was conducted from the winter of 1987 until September of 1988.

The impetus for the transonic HLFC experiment was the perception that HLFC concepts could provide higher efficiency (laminar area achieved per unit mass flow required and weight of the suction system) and fewer installation problems than any near-full-chord or full-chord transonic LFC concept. HLFC calculations made in the mid-seventies at transonic speeds using the STAYLAM stability and boundary layer codes[13] and the BGK airfoil code[14] by the first author; exper-

iments by John Allen of McDonnell-Douglas Aircraft Company around 1984 on a model with a perforated leading edge; and the success of Dr. W. Pfenninger and his associates in the late 1950's in suction-assisted, laminar-flow subsonic experiments in the NASA Ames 12-ft Pressure, University of Michigan 5 × 7-ft and Norair 7 × 10-ft Wind Tunnels[15–16] all added conviction to the perception. In addition, simulated hybrid experiments were conducted on the slotted and perforated LFC models at transonic speeds in the 1984-1987 time period. These simulated hybrid experiments demonstrated the ability of a suction surface to maintain laminar flow well beyond the point where suction was terminated at transonic speeds. This was accomplished despite the fact that the pressure distribution beyond the suction cut-off point was adverse and the slots or holes (perforated surface) were not sealed and smoothed.

The HLFC model utilized in the present tests employed the same lower surface, slotted-suction panels and forward (0 to 25% chord) upper-surface, perforated-suction panel as for the LFC tests. However, new solid middle and aft upper surface panels were constructed with contours designed to achieve a favorable pressure gradient from approximately 20% to 60% of the chord at a Mach number of 0.811. The chord and sweep were maintained at approximately 7 feet and 23 degrees, respectively, and the suction system, instrumentation, and wind tunnel liner remained essentially as they were for the LFC experiment.

In the present paper, the methods/codes used to develop the contour of the HLFC upper surface will be briefly outlined followed by a discussion of the airfoil model, suction system, instrumentation, and some example results from the wind tunnel tests. The last section will contain some concluding remarks.

Nomenclature

Symbols

a	local speed of sound
a_∞	speed of sound in free stream
c	airfoil chord
c_d	section drag coefficient, $= \frac{\text{drag force}}{\frac{1}{2}\rho_\infty U_\infty^2 c}$
$c_{d,s}$	suction drag coefficient
$c_{d,w}$	wake drag (total of skin friction, shock and form drags)
c_l	lift coefficient, $= \frac{\text{lift force}}{\frac{1}{2}\rho_\infty U_\infty^2 c}$
C_p	pressure coefficient, $= \frac{p-p_\infty}{q_\infty}$
C_Q	coefficient of suction, $= \frac{\rho_w w_w}{\rho_\infty U_\infty}$
M	local Mach number u_∞/a
M_∞	free stream Mach number, $= \frac{U_\infty}{a_\infty}$
p	pressure
Δp_t	$= p_t - p_{t_\infty}$
q_∞	free stream dynamic pressure, $= \rho_\infty U_\infty^2/2$
$\overline{R}$	Reynolds number based on boundary layer edge conditions and displacement thickness in transformed plane (see References 19 and 21)
R_c	Reynolds number based on chord, $= \frac{\rho_\infty U_\infty c}{\mu_\infty}$
u, v, w	velocity components in x, y and z directions
$\tilde{u}$	RMS value of x component of fluctuating velocity
U_∞	free stream velocity
x	distance measured in streamwise direction
y, z	cartesian coordinates normal to x; z also used to indicate distance along wake and boundary-layer rakes
α	angle of attack
Λ	sweep angle
ρ	density

Abbreviations

ACEE	NASA's Aircraft Energy Efficient Program
HLFC	hybrid laminar flow control
LaRC	NASA Langley Research Center
LFC	laminar flow control
N.F.	leading edge normal flow
NLF	natural laminar flow
S.F.	spanwise flow
8-ft TPT	NASA Langley 8-ft Transonic Pressure Tunnel

Subscripts

inst	instantaneous value
n	normal to the leading edge
s	suction component
SUC	extent of suction
t	total or stagnation pressure conditions
tot	total value, suction plus wake drag
TR and trans	value at transition
	free stream condition or in free stream direction
w	wake component of drag
e	edge of boundary layer
S	sonic value
us	value for upper surface
ls	value for lower surface
bl	quantity based on boundary-layer-rake measurements

II. Design of HLFC Upper-Surface Contour

Precursor Studies

As noted in the Introduction, a number of separate calculations and experiments provided data indicating

that a transonic hybrid-laminar-flow-control (HLFC) concept might be much more efficient than an LFC one in terms of the extent of laminar flow obtained for a given amount of suction mass flow. Parametric analytical studies were carried out using various boundary-layer-stability codes and the results fed into an analysis by Goradia who provided final geometry and suction requirements for the HLFC upper surface.

During the time that the analytical parametric studies were being carried out tests were conducted using the LFC slotted- and perforated-surface models simulating HLFC concepts. These tests showed that substantial runs of laminar flow could be achieved beyond the point where suction was terminated even though the pressure distributions obtained on these models were not well-suited to HLFC.

Constraints and Goals

The determination of the final geometry and pressure distribution for the upper surface of the HLFC airfoil was carried out with the following constraints:

- The upper forward perforated suction-panel of the perforated-surface LFC model had to be used (see References 9-11).
- The geometry of the new solid mid and aft upper-surface panels had to fair smoothly into the existing forward upper-surface panel and the trailing edge flaps.
- Laminar flow was desired back to 60% of the chord.
- The supersonic bubble aspect ratio must be smaller than that on the LFC model.
- Utilization of the existing wind-tunnel-wall contoured liner was required.
- Flow separation should remain beyond $x/c > 0.95c$.
- The model chord was to remain at 7.07 ft.
- The sweep of the model was to remain at 23 deg.
- Suction was to be utilized on the lower surface back to 84% of the chord for all tests in order to maintain attached flow to the maximum extent possible.

No attempt was made to design for a specific value of c_l although the value that evolved, 0.48, was very close to the design c_l for the LFC airfoil. Design Mach number was reduced slightly from 0.82 to 0.81 and the Reynolds number of the design point was chosen as 15 $\times 10^6$ based on the streamwise chord. A much more ambitious design would have been attempted had the above constraints not existed.

Analytical Methods

The methods used for the final design of the upper surface contour of the HLFC model are documented in a number of papers. Specific methods and their uses are listed below:

- Airfoil Top-Surface Contour Determination
  - Perturbation method of characteristics for inverse design at transonic speeds [17].
  - Bauer-Garabedian-Korn program for transonic analysis [14].
  - NASA-Lockheed multi-component airfoil program for subsonic analysis [18].
- Detailed Boundary Layer Analysis, Stability Calculations and Separation
  - Integral compressible laminar boundary layer with sweep, suction, and chordwise and spanwise pressure gradients at subsonic, transonic, and supersonic Mach numbers [19, 20, and 21].
  - Short bubble and reattachment criteria [22].
  - Instability and transition prediction due to Normal Flow (N.F.) and Spanwise Flow (S.F.) including the effects of spanwise pressure gradients [20].
  - Separating turbulent boundary layer method for subsonic and transonic speed [23]. This method was extended to handle infinitely swept wings for the HLFC design.
- Drag Computations
  - Methods for computing $c_{d,w}$ and $c_{d,s}$ for infinitely swept wings and bodies of revolution at Mach numbers from subsonic through supersonic [21].

The governing boundary layer equations (see e.g. Reference 19) are solved in a transformed plane (Stewartson transformation). Velocity and temperature profiles are derived for the leading-edge-normal (N.F.) and spanwise flow (S.F.) directions in the transformed plane using an integral-equation approach. These

same profiles are then used in an "extended" Orr-Somerfeld stability analysis in the transformed plane to determine the point of instability and transition. The "extension" of the incompressible Orr-Somerfeld stability equation was accomplished through the use of dimensional analysis and the laws of dynamic similarity. Transition is determined with the aid of the empirically based curve for $\overline{R}_{tran} - \overline{R}_{inst}$ vs. $\frac{\bar{u}}{U_\infty}$ where $\overline{R}_{tran}$ and $\overline{R}_{inst}$ are determined in the transformed plane. Transition locations in the physical plane due to N.F. and S.F. instabilities are obtained with the aid of inverse-transformation boundary-layer parameters.

In order to check the ability of the system of codes just listed to predict N.F. and S.F. transition, a number of validation calculations were carried out and documented for configurations where data already existed. They include:

- Boltz's variable sweep wing with NACA 64_2A015 section [24]
- Phoenix wing [25]
- NASA-LaRC LFC wing [9-11]
- F-14 laminar wing glove [26]

for subsonic and transonic speeds and the

- AEDC cone [27-28]

for transonic and supersonic speeds.

A number of calculations for configurations where only supersonic data is available were made and presented in Reference 29. Since the HLFC tests were only run at subsonic and transonic speeds, the validations using the data for the LFC wing in the 8-ft TPT and the F-14 laminar wing glove in flight are particularly significant.

HLFC Airfoil Contour and Pressure Distribution

The airfoil shape and pressure distribution finally determined, subject to the constraints previously described, are given in Figures 1 and 2. Figure 1a shows a comparison of the actual shapes of the HLFC and LFC airfoils; Figure 1b shows the same comparison but with the ordinate amplified by a factor of 5 to better show the differences. A lower suction peak relative to that for the LFC airfoil was utilized to reduce the size of the supersonic bubble and permit a favorable pressure gradient to about 55% chord (Figure 2). This was accomplished not only by the contour modification but by reducing the design angle of attack and Mach number (from 0.82 to 0.811). In addition a trailing edge flap deflection of 4.7° was required to achieve the desired pressure level and distribution.

The 2-D supersonic bubble associated with the design HLFC pressure distribution is shown in Figure 3 along with the two and three-dimensional bubbles for the LFC airfoil. Clearly, the supersonic bubble for the HLFC upper surface is much smaller in extent than that for the LFC. Also shown on the figure are the boundaries of the corner fillets for the streamline liner in the test section.

Normal-flow and spanwise-flow transition calculations carried out for the HLFC upper surface using the methods of Reference 19 are depicted in Figure 4. Generally, the neutral points are between $x/c = 0$ and 0.1 for the range of Reynolds numbers indicated. For Reynolds numbers up to 16×10^6 the N.F. instability causes transition to occur at $x/c = 0.57$; beyond this Reynolds number the S.F. instability dominates causing transition to move steadily forward as Reynolds number increases. Turbulent separation is predicted to occur at $x/c = 0.95$ (curve at top of Figure 4) for the range of Reynolds numbers shown.

Upper-Surface Suction Requirements

The predicted suction mass-flow requirements for the design point correspond to a C_Q of approximately $- 0.3 \times 10^{-3}$ over the first 25% of the chord at $R_c = 15 \times 10^6$. As expected, this is a higher level than that required for the LFC concepts where suction extends over most of the chord. The suction coefficient as a function of Reynolds numbers is shown in Figure 5 (Reference 19).

Upper-Surface Drag

Calculated suction- and wake-drag coefficients for the upper surface of the HLFC model versus free stream Reynolds number are plotted in Figure 6. It is evident from this figure that the suction-drag coefficient decreases with increasing Reynolds number and is less than one drag count (< 0.0001) over the Reynolds number range plotted. The wake drag coefficient on the other hand ranges from 0.0028 to 0.0038, the latter value occurring at a Reynolds number of 30×10^6. The predicted suction drag is clearly a small fraction of the total drag.

III. Model, Wind, Tunnel, Suction System, and Instrumentation

Detailed discussions of the LFC model construction, the wind tunnel and the modifications made to it to

improve the uniformity and quality of the flow over the model, the various types and locations of the instrumentation, and the system used for boundary layer suction through the model surface are given in References 4 through 11. Only a brief review of these items will be given here.

HLFC Model

The model used for the HLFC tests was the same in most respects as that used for the tests of the LFC perforated-surface model. The primary differences were occasioned by the replacement of the middle and aft upper-surface porous panels by solid panels with the geometry shown in Figure 1 and a few suction system modifications. The bottom surface of the HLFC model was comprised of the same slotted-suction panels as the LFC model. Figure 7 illustrates the panel arrangement used in the HLFC model. The forward, upper-surface, perforated panel extended from the leading edge to 25.7% of the chord and the two solid upper-surface panels extended from 25.7% to 58.6% and 58.6% to 89.1% of the chord. The trailing edge flaps made up the remaining 10.9% of the chord.

Construction features of the perforated (also referred to as porous) and slotted surfaces can be seen in the sketches of Figure 8. The perforated panel has an aluminum substructure which forms the walls of the main ducts (see Figure 8a). Plenum ducts are made of fiberglass, graphite, and carbon fiber cloth as indicated in Figure 8b. As evident in Figure 10a every other plenum duct is inactive and contain no metering holes. The surface itself is made of titanium with electron beam drilled holes which were nominally 0.0026 inches in diameter at the outer suction-flow surface and slightly larger on the outflow or bottom-side surface. The titanium material was 0.025 inches thick and the hole spacing was also 0.025 inches. The surface of the material was smooth to the touch and expected to be aerodynamically smooth in the regions where the pressure difference across the surface was zero. A detailed discussion of the design and construction of the perforated panels can be found in Reference 5.

The slotted suction panels were much more rugged in construction than the perforated ones (see Figure 8c). The substructure was machined out of a solid aluminum billet and the aluminum surface bonded to it. Slots were subsequently cut with jewelers circular saw blades. Slot widths ranged from 0.002 to 0.0063 inches with the smaller widths near the leading edge.

Wind Tunnel

The HLFC (as well as the LFC) tests were carried out in the Langley Research Center 8-foot Transonic Pressure Tunnel (8-ft TPT) which has a Mach number capability from approximately 0.2 to 1.3 (without the required contoured liner) and can be pumped down or pressurized to run at sub-atmospheric or above atmospheric pressures. At the design Mach number, Reynolds number could be varied from 9×10^6 to 24×10^6 based on the chord of the model (7.07 ft).

Prior to the start of the LFC tests the 8-ft TPT was modified by the installation of 5 screens and a honeycomb in the plenum just upstream of the contraction and test section (see Figure 9a). These devices were aimed at improving the flow quality in the test section and thus achieve transition locations on the model more like those obtainable in free air. References 3 and 4 describe these modifications in considerable detail.

Another substantial modification to the tunnel was the installation of a streamline liner starting in the contraction, continuing through the test section, and terminating in the high speed diffuser. It was designed to provide the same flow about the LFC model in the wind tunnel as that about an infinite-span, 23° swept wing of constant chord in free air. Since the wing was swept and lifting, the liner on all four walls was different. Figure 9a gives a sketch of the contraction and test section of the 8-ft TPT showing the screens, honeycomb, and liner. Also shown in the sketch is the sonic throat or choke which was an integral part of the liner. This choke was effective in reducing the upstream propagation of acoustic disturbances providing a further improvement in the test section flow quality (see Reference 11). A photograph of the model installed in the test section is provided in Figure 9b. One of the chokes can be seen on the wall to the left and downstream of the model. Reference 6 describes in detail the design of the streamline liner.

Suction System

Certainly the most complicated of the HLFC test equipment was the suction system. The main components are shown schematically in Figure 10. Figure 10a shows the installation of the suction nozzles in the end of the model nearest the floor. Separate suction nozzles are provided for the turbulent zone adjacent to the wall since this region is separated by a bulkhead from the laminar region (see Figure 10a). The bulkhead provides a barrier for the noise emanating from the turbulent boundary layer on the airfoil surface in the turbulent zone from propagating through the holes and ducts into the laminar ducts in the mid-span region of the model. In addition, the suction levels in the turbulent zones at each end of the model are considerably higher (see Reference 4) than in the laminar regions on the top and bottom surface. Figure 10b is provided to show the flow on the surface and the

turbulent zones at each end of the model emanating from the junctures of the airfoil model with the liner. A similar flow situation exists on both the top and bottom surfaces.

Prior to the HLFC tests additional suction nozzles were installed in the forward, upper-surface perforated panel so that each duct had a suction nozzle at both ends. (In the earlier LFC tests a number of ducts had only one nozzle.) Also the suction hoses which connected the suction nozzles to the suction control boxes (discussed later) were enlarged. Finally two additional vacuum pumps with much higher pressure ratios than those used in the earlier LFC experiment were installed to provide suction for the forward upper surface panel.

The suction control system is shown in the sketch of Figure 10c. Hoses from the suction nozzles at both ends of the airfoil are connected to one of five airflow control boxes. Each nozzle fitting has its own valve internal to the control box for adjusting the mass flow in that hose. All control boxes were equipped with sound suppressing material and screens to reduce the sound and vorticity levels and thus minimize the levels of the disturbances propagated upstream to the airfoil.

Each control box is connected to a common manifold through a controllable sonic nozzle. As in the case of the flow quality treatment of the control boxes the sonic nozzles are intended to minimize or prevent acoustic disturbances from the collector manifold and suction compressors from propagating upstream. The collector manifold and the 10,000-cfm compressors (4.5:1 compression ratio) can readily be seen in Figure 10c. Flow from the downstream end of the 10,000-cfm pumps is returned to the tunnel through the trailing edge of hollow turning vanes at the end of the high speed diffuser. Not shown in the sketch of Figure 10c are the two Stokes pumps, with a compression ratio of approximately 7:1, which were added to provide suction to the top forward panel of the model, particularly in those ducts nearest the leading edge where the lowest surface pressures (in the area where suction was applied) were encountered.

Additional details of the suction system can be found in References 4 and 11.

Instrumentation

The number of static pressure gages/orifices associated with the airfoil, liner, suction nozzles, ducts, and wake rake are listed in Figure 11 (from Reference 11). Also given are the number of thin-film and acoustic gages that were utilized. The pressure orifices on the airfoil were used to obtain longitudinal pressure distributions at a number of spanwise stations on the upper and lower surfaces of the airfoil. Wake rake pressure measurements were used to obtain the airfoil wake drag. Pressure measurements in the ducts were used to control the suction mass flow level and distribution through the ducts and surface of the airfoil. Finally static pressures were measured on the liner to determine whether the supersonic bubbles above and below the airfoil surface extend to the liner, whether the flow was uniform across the tunnel at the end of the contraction, and to determine the freestream Mach number ahead of the airfoil.

Figure 12 shows the location of the pressure orifices as well as the acoustic and thin film gages on the upper surface of the model. The lower surface was similarly equipped. Dynamic instrumentation (acoustic and thin-film gages) was used to determine the disturbance levels in the ducts and on the model surface or, in the case of the thin films, whether the flow was laminar, transitional, or turbulent. A more detailed discussion of the data reduction system as well as the wall-liner and wake-rake pressure instrumentation is given in References 4, 9, and 11.

IV. HLFC Test Results

The quantities that could be varied in the HLFC experiment included Mach number, Reynolds number, suction level and suction extent. A discussion will be given in the following sections of the effect of varying these quantities facilitated primarily by pressure-distribution, transition-location, and drag data plots.

Mach Number Effects

Three different types of pressure distributions were obtained on the upper surface of HLFC airfoil as Mach number was increased from 0.80 to 0.826 and are termed for convenience of discussion Type 1, 2 and 3 distributions. As seen in Figure 13, the closest agreement between the design pressure distribution and experimental data was at Mach numbers in the vicinity of 0.82 (Type 2). At this Mach number the adverse gradient following the suction peak near the leading edge is much steeper and occurs over more of the chord than that of the design pressure distribution. The chordwise extent of the favorable pressure gradient obtained experimentally is less than design but the gradient itself is larger. The pressure recovery beyond an x/c of 0.55 is in good agreement with theory as are the pressure distributions on the bottom side pressures. Even better agreement of the bottom side pressures is obtained as Reynolds number is reduced from the 15×10^6 value applicable to Figure 13.

Mach numbers in the vicinity of 0.8 (Type 1) provide more positive pressure coefficients than design on both

the top and bottom surfaces (see Figure 13). Pressure coefficients at a Mach number of 0.826 (Type 3) on the other hand are more negative (higher suction pressures) than the design values over most of the top and bottom surfaces. In addition a favorable gradient was obtained on the top surface beyond the point where the pressure recovery was designed to start. Most of the discussion in this paper will be concentrated on results obtained with Types 2 and 3 pressure distributions.

The extent of laminar flow obtained on the upper surface of the model for the three Mach numbers of Figure 13, and with suction to 25% of the chord, is shown in Figure 14. The longest run of laminar flow was obtained at the highest Mach number near the bottom of the airfoil while the most uniform spanwise distribution of laminar flow across the span was obtained at the lowest Mach number. These results (Figure 14) generally reflect the extent of the favorable pressure gradient on the top surface of the HLFC model.

Velocity profiles obtained from the boundary layer rake, attached to the top surface near the model centerline at 95% of the chord, for the same Mach numbers listed on Figure 13 are plotted in Figure 15. The character of the curves indicate that the flow is attached at this chordwise location at all three Mach numbers. However, there is an indication from the wake rake total-pressure-difference profiles of Figure 16 that at a Mach number of 0.826 flow separation is occurring aft of 0.95c.

Drag coefficients ($c_{d,bl}$), based on the boundary layer velocity profiles obtained at 0.95c, are tabulated on the right side of Figure 15. Obviously these drag coefficients are lower than those for the entire upper surface. With the aid of the wake rake profiles of Figure 16, total upper surface wake-drag coefficients have also been estimated and tabulated on Figure 15.

As noted earlier, the total-head pressure-difference $\Delta p_t (\equiv p_t - p_{t_\infty})$ wake profile normalized by the free stream dynamic pressure is plotted in Figure 16. Negligible differences are seen in the top surface total-head defect between the curves for $M = 0.805$ and 0.822 while there is a small difference for the bottom surface ($z < 3.0$ in). Much larger differences are seen between the curves for the lower two Mach numbers and that for $M = 0.826$, particularly on the bottom where flow separation in the aft cove has occurred at $M = 0.826$. This phenomena can also be inferred from the wake drag coefficients tabulated on the figure and from the bottom surface pressures given in Figure 13.

Top surface and total drag coefficients, as well as transition locations, as a function of Mach number for a Reynolds number of 10×10^6 are given in Figure 17. At the low Mach numbers the top surface contributes about two thirds of the wake drag while at Mach numbers greater than 0.8 it is down in the 50 to 60% range. Top surface wake-drag levels range from 0.0017 at $M_\infty = 0.4$ to 0.0025 at $M_\infty = 0.81$. Transition moves forward as Mach number is increased from 0.4 and remains at about 60% of the chord for $M_\infty > 0.6$ until a Mach number of approximately 0.822 is exceeded. At this condition the pressure changes from Type 2 to Type 3 and transition moves rapidly to 90% of the chord. While there is a decrease of 5 or 6 drag counts at this Reynolds number when the pressure distribution changes from Type 2 to Type 3, more of a difference might have been expected based simply on transition location.

Reynolds Number Effects

Reynolds number (R_c) was varied from approximately 9×10^6 to 24×10^6 for the three types of pressure distribution illustrated in Figure 13.

Type 1 and 2 transition locations are very little affected by Reynolds number changes while those for Type 3 vary significantly (see Figure 18). Over the Reynolds number range of Figure 18, i.e., 9×10^6 to 24×10^6, transition for Type 3 pressures ($M \approx 0.826$) moved from 90% chord forward to 50% chord.

Drag coefficients obtained from the boundary layer rake located at $x/c = 0.95$ are plotted in Figure 19 for the same range of Reynolds number as Figure 18. The trends shown on this figure are not entirely consistent with the transition data (Figure 18) and this is due to the combined effects of flow separation and the movement of transition. Minimum drag levels occur near $R_c = 15 \times 10^6$ which is the design Reynolds number. Flow separation is seen to have the most effect for Reynolds numbers beyond 17×10^6 and a Mach number of 0.826. Increasing drag levels between Reynolds numbers of 22 and 24×10^6 are due primarily to the forward movement of transition. It must be remembered that as the Reynolds number is increased in the wind tunnel at a constant Mach number the disturbance level in the wind tunnel also increases.

Extent-of-Suction Effects

The extent of suction on the upper surface was varied from zero to 25% of the chord by adjusting individual duct pressures to the same values as the local surface pressure and thus inhibiting flow through the surface. Figure 20 shows the Type 2 pressure distributions which result from four different extents of suction from 5 to 25% of the chord. Full suction back to 85% of the chord on the lower surface was maintained for all conditions. The Reynolds and Mach numbers of these data are 15×10^6 and 0.82, respectively. Note

that the pressure distributions change very little with the extent of suction; there is, however, an increase in pressure coefficient over the middle portion of the lower surface as the extent of suction is increased. It can also be seen that the flow is separated in the rear cove on the bottom surface in all cases. All four top-surface pressure distributions have the same shape and indicate the possibility of a shock induced separation bubble beyond $x/c = 0.65$. In addition, the flow appears to separate near the trailing edge at $x/c \approx 0.95$.

Boundary layer velocity profiles at $x/c = 0.95$ for the four suction-extent cases of Figure 20 are plotted in Figure 21. It is evident from this figure that the boundary layer at this location becomes thicker and the drag increases as the extent of suction is reduced. Wake-rake profiles, Figure 22, indicate the same trend with the most pronounced changes on the top side. These changes are caused by the forward movement of transition as shown in Figure 23. Note from this figure that suction applied to the last duct near the 25% chord location had little effect on the extent of laminar flow achieved. The additional suction was simply insufficient to move the transition point any further into the adverse pressure region beyond $x/c \approx 0.60$.

The variation of the various drag components with the extent of suction is given in Figure 24. Also plotted in Figure 24 is the variation of the lift coefficient with the extent of suction. The most important curve on this figure is that for the estimated top-side drag coefficient ($c_{d,w,us}$). With no suction, the top-side drag coefficient is about 40 counts ($c_{d,w,us} = 0.0040$) while, with suction applied back to 21% of the chord, the drag coefficient is 23 counts. Note from Figure 6 that the predicted wake drag coefficient for the top surface with suction to 25% of the chord was 27 counts.

Level-of-Suction Effects

Decreasing the level of suction from its nominal value at a Reynolds number of 15×10^6 and a Mach number of approximately 0.82 (Type 2 pressure distribution) has an effect similar to that of decreasing the extent of suction. Suction level was reduced in two ways, one by the uniform reduction of suction on all the ducts and the other by closing down individual ducts in the most uniform manner possible. Drag levels for the latter type of suction mass-flow reduction as a function of the percent of the normal suction level were about the same as for uniform suction reductions. Figure 27 compares $c_{d,bl}$ and $c_{d,w}$ for both methods of reducing suction. Also shown are the estimated $c_{d,w,us}$ values for the uniform suction reduction tests. It is clear from the figure that for equal amounts of suction ($c_{d,s,us}$) similar drag values are provided by the top surface, and the entire airfoil, for both suction-reduction approaches. Finally, a suction level of 100% reduces upper surface wake drag relative to that for zero suction by about 40%.

It should be noted that the increments in wake drag coefficient due to the bottom surface, $c_{d,w,ls} = c_{d,w} - c_{d,w,us}$, varies from about 30 to 40 counts. These levels are high, even though there is substantial suction on the lower surface, due to the fact that the flow in the aft cove of the bottom surface is separated. At a Reynolds number of 9×10^6 ($M_\infty \approx 0.82$), where the flow is attached in the aft cove region, bottom side wake drag coefficients are on the order of 0.0020.

Comparison of HLFC with LFC Results

It was noted in the Introduction that the HLFC experiment followed the LFC experiment in the 8-ft TPT. Indeed, most of the same equipment and airfoil model used in the LFC tests were employed in the HLFC experiment. The primary modification, as noted earlier, was the replacement of the middle two panels of the upper surface of the LFC model with solid panels having a slightly different contour. The first 25.7% of the upper surface was the perforated panel employed in the LFC experiment; the lower surface was comprised of the slotted panels used in the LFC experiment (see Figure 7). Results of the research on the slotted LFC model are documented in References 9 and 11.

A comparison of the transition locations, based on the most forward location in the test region, for the HLFC and slotted LFC models are given in Figure 26. The LFC model is seen to have laminar flow over near 100% of the chord at 10 million chord Reynolds number and this decreases to about 61% of the chord for $Re_c = 15 \times 10^6$ and beyond. The HLFC model on the other hand had laminar flow back to about 59% of the chord over the Reynolds number range plotted. Drag-coefficient data for the same conditions shows a similar trend. At low Reynolds numbers, the LFC drag coefficient is much lower (about half) than that for the HLFC while beyond a Reynolds number of 15×10^6 the two are comparable.

V. Conclusions

The following conclusions refer to the calculations and data for the top surface of the HLFC model. The bottom surface of the HLFC was the same as for the slotted LFC model and was not a variable in the experiment. It should be recognized however that the flow over the bottom surface did influence that over the top, and vice versa, particularly when there was flow separation near the trailing edge of either surface.

1 Large extents of laminar flow were achieved with small total suction mass flows.

2 Pressure distributions appropriate to HLFC concepts were achieved.

3 Top surface drag coefficients with suction extending from near the leading edge to 20% of the chord were about 40% lower than those obtained with no suction.

4 While laminar flow was achieved back to 90% of the chord in some cases the associated drags were not as low as expected due to flow separation near the trailing edge.

5 Reducing the extent of suction to less than twenty percent of the chord caused a rapid forward movement of transition and increase in drag.

6 Decreasing the level of suction below eighty percent of the nominal level caused a rapid increase in drag.

7 Drag coefficients for the Type 1 and 2 pressure distributions were less affected by Reynolds number changes than those for Type 3.

8 The extent of laminar flow decreased and drag coefficients increased as Mach number increased except when the Mach number was increased from 0.82 to 0.825 where there was an abrupt increase in the extent of laminar flow.

9 Transition locations and drag coefficients for the HLFC surface beyond a chord Reynolds number of 15×10^6 were comparable to those obtained for the LFC model with full chord suction.

10 On the basis of the present tests it appears that HLFC airfoils and wings can be designed for transonic speeds with lift and drag coefficients approaching those of LFC designs.

Acknowledgement

This research was supported by the National Aeronautics and Space Administration under NASA Contract No. NAS1-18605 while the first author was in residence at the Institute for Computer Applications in Science and Engineering, NASA Langley Research Center, Hampton, VA 23665.

References

[1] Aircraft Fuel Conservation Technology - Task Force Report. OAST NASA, September 10, 1975. (Available as NASA TM X-74295).

[2] Jones, G. S.; Stainback, P. C.; Harris, C. D.; Brooks, C. W.; and Clukey, S. J.: Flow Quality Measurements for the Langley 8-Foot Transonic Pressure Tunnel LFC Experiment. 27th Aerospace Sciences Meeting, Reno, NV, January 9-12, 1989, AIAA Paper No. 89-0150.

[3] Harris, C. D.; and Brooks, C. W., Jr.: Modifications to the Langley 8-Foot Transonic Pressure Tunnel for the Laminar Flow Control Experiment. NASA TM-4032, 1988.

[4] Harris, Charles D.; Harvey, William D.; and Brooks, Cuyler W., Jr.: The NASA Langley Laminar-Flow-Control Experiment on a Swept, Supercritical Airfoil, *Design Overview*, NASA TP-2809, May 1988.

[5] Maddalon, Dal V.; and Poppen, William A., Jr.: Design and Fabrication of Large Suction Panels with Perforated Surfaces for Laminar Flow Control Testing in a Transonic Wind Tunnel. NASA TM-89011, 1986.

[6] Newman, Perry A.; Anderson, E. Clay; and Peterson, John B., Jr.: Aerodynamic Design of the Contoured Wind-Tunnel Liner for the NASA Supercritical, Laminar-Flow-Control, Swept-Wing Experiment. NASA TP-2335, September 1984.

[7] Berry, S.; Dagenhart, J. R.; Brooks, C. W., Jr.; and Harris, C. D.: Boundary-Layer Stability Analysis of LaRC 8-Foot LFC Experimental Data. NASA CP-2487, Part 2, March 1987.

[8] Brooks, C. W., Jr.; Harris, C. D.; and Harvey, W. D.: The NASA Langley Laminar-Flow-Control Experiment on a Swept Supercritical Airfoil – *Drag Equations*. NASA TM-4096, February 1989.

[9] Harris, C. D.; Brooks, C. W., Jr.; Stack, J. P.; and Clukey, P. G.: The NASA Langley Laminar-Flow-Control Experiment on a Swept Supercritical Airfoil – *Basic Results for Slotted Configuration*. NASA TM-4100, June 1989.

[10] Harvey, W. D.; and Pride, J. D.: The NASA Langley Laminar Flow Control Experiment. AIAA Paper No. 82-0567, 1982.

[11] Bobbitt, P. J.; Harvey, W. D.; Harris, C. D.; and Brooks, C. W., Jr.: The Langley 8-Ft Transonic

Pressure Tunnel Laminar-Flow-Control Experiment – Background and Accomplishments. Natural Laminar Flow and Laminar Flow Control, M. Y. Hussaini and R. W. Barnwell (Editors), Springer-Verlag, 1991.

[12] Bobbitt, P. J.; Waggoner, E. G.; Harvey, W. D.; and Dagenhart, J. R.: A Faster "Transition" to Laminar Flow. SAE Paper 851855, October 14 - 17, 1985.

[13] Carter, J. E.: A Fortran Program for the Suction Transition Analysis of a Yawed Wing Laminar Boundary Layer. NASA TMX-74013, March 1977.

[14] Bauer, Frances; Garabedian, Paul; Korn, David; and Jameson, Antony: Supercritical Wing Sections II. Volume 108 of Lecture Notes in Economics and Mathematical Systems, Springer-Verlag, 1975.

[15] Lachmann, G. V. (Editor): Boundary Layer and Flow Control, Volume 2. Pergamon Press, 1961.

[16] Pfenninger, Werner: Laminar Flow Control Laminarization. Special Course on Concepts for Drag Reduction, AGARD-R-654, June 1977, pp. 3-1 to 3-75.

[17] Goradia, S. H.: The Method of Characteristics Perturbation Technique as Applied to Airfoil Design. Lockheed-Georgia Company Advanced Design Aerodynamics Memorandum 13-68, March 1968.

[18] Stevens, W. A.; Goradia, S.; and Braden, J. A.: Mathematical Model for Two-Dimensional Multi-Component Airfoils in Viscous Flow. NASA CR-1843, 1971.

[19] Goradia, Suresh H.; and Morgan, Harry L.: Theoretical Methods and Design Studies for NLF and HLFC Swept Wings at Subsonic and Transonic Speeds. Natural Laminar Flow and Laminar Flow Control Symposium, NASA CP 2487, Part 2, Hampton, VA, March 16-19, 1987.

[20] Goradia, S. H.; Bobbitt, P. J.; Morgan, H. L.; Ferris, J. C.; and Harvey, W. D.: Results of Correlations for Transition Location on a Clean-Up Glove Installed on an F-14 Aircraft and Design Studies for a Laminar Glove for the X-29 Aircraft Accounting for Spanwise Pressure Gradient. Proceedings of a Symposium held at NASA Langley Research Center, NASA CP 3020, Vol. II, April 19-21, 1988.

[21] Goradia, S. H.; Bobbitt, P. J.; Ferris, J. C.; and Harvey, W. D.: Theoretical Investigations and Correlative Studies for NLF, HLFC, and LFC Swept Wings at Subsonic, Transonic, and Supersonic Speeds. SAE Paper 871861.

[22] Goradia, S. H.; and Lyman, V. L.: Laminar Stall Prediction and Estimation of $C_{L_{max}}$. Journal of Aircraft, Vol. II, No. 9, September 1974, pp. 528-536.

[23] Goradia, S. H.; and Morgan, H. L.: A New, Improved Method for Separating Turbulent Boundary Layer for Aerodynamic Performance Prediction of Trailing Edge Stall Airfoils. Paper presented at AIAA 4th Applied Aerodynamics Conference, Paper 86-1832-CP, June 9-11, 1986, San Diego, CA.

[24] Boltz, F. W.; Kenyon, G. C.; and Allen, C. Q.: Effects of Sweep Angle on the Boundary-Layer Stability Characteristics on an Untapered Wing at Low Speeds. NASA TN D-338, October 1960.

[25] Raspet, A.; and Gyorgyfalvy, D.: Boundary-Layer Studies on Phoenix Sailplane. Presented at VIII Congress of O.S.T.I.V., Köln, Germany, June 1960.

[26] Meyer, R. R.; Trujillo, B. M.; and Bartlett, D. W.: F-14 VSTFE and Results of the Clean-Up Flight Test Program. NLF and LFC Research Symposium, NASA Langley Research Center, NASA CP 2487, March 16-19, 1987.

[27] Goradia, S. H.; Bobbitt, P. J.; and Harvey, W. D.: Computational Results for the Effects of External Disturbances on Transition Location on Bodies of Revolution from Subsonic to Supersonic Speeds and Comparisons with Experimental Data. Aerospace Technology Conference and Exposition, Anaheim, CA, September 25-28, 1989, SAE Technical Paper Series 892381.

[28] Dougety, N. S., Jr.; and Fisher, D. F.: Boundary Layer Transition on a 10-Degree Case. AIAA-8-0154, 1980.

[29] Goradia, S. H.; and Bobbitt, P. J.: Theoretical Investigation for the Effects of Sweep, Leading Edge Geometry and Spanwise Pressure Gradients on Transition and Wave Drag at Transonic and Supersonic Speed with Experimental Correlations. SAE Paper 881484, 1988.

[30] Corke, T. C.: Three-Dimensional Mode Resonances in Boundary Layers, Jets, and Wakes. Volume I - Instability and Transition. M. Y. Hussaini and Robert G. Voigt (Editors), Springer-Verlag, 1990.

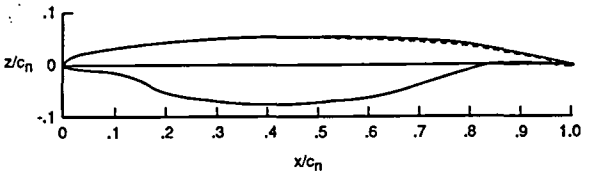

(a) Actual geometry.

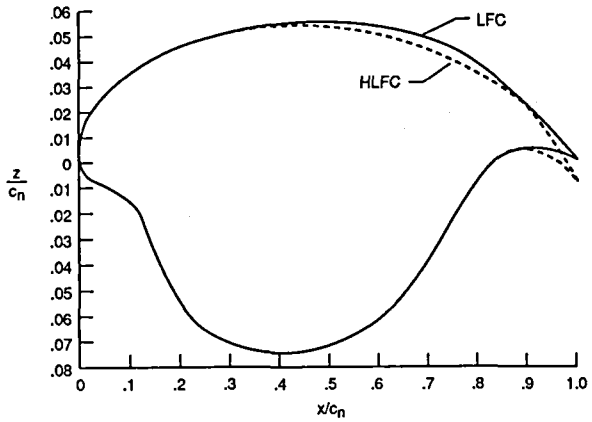

(b) Geometries with vertical scale amplified.

Figure 1. Geometries of HLFC and LFC airfoils.

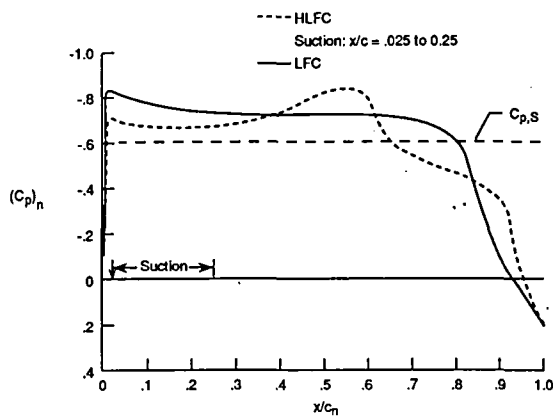

Figure 2. Comparison of the design pressure distributions for the HLFC and LFC models. $\Lambda = 23°$.

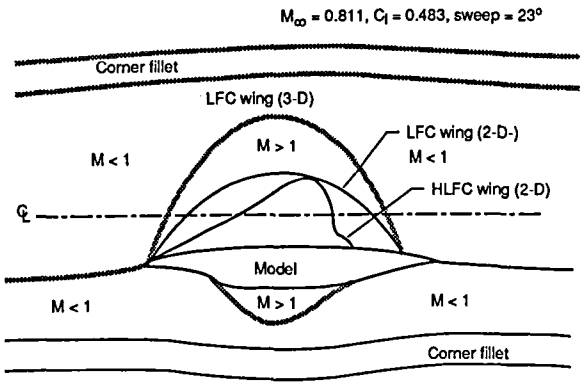

Figure 3. Comparison of streamwise supersonic bubble shapes for HLFC and LFC airfoils at their design conditions.

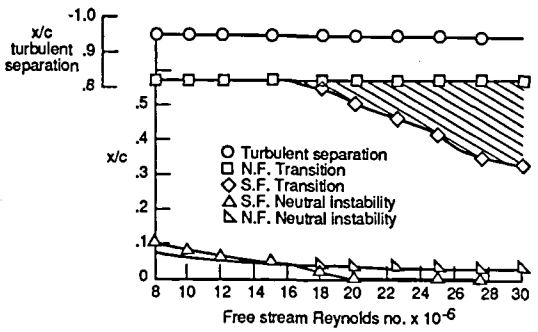

Figure 4. C-F and N-F stability calculations as well as prediction of location of turbulent separation for top surface of HLFC airfoil. $M_\infty = 0.811$, $c_l = 0.483$, and $\Lambda = 23°$.

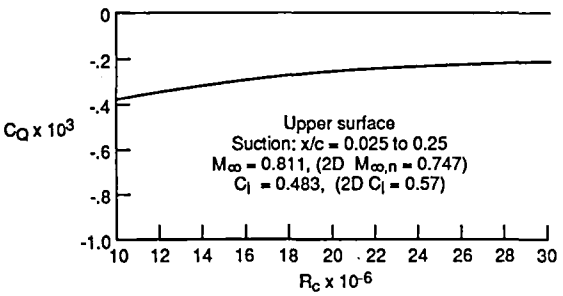

Figure 5. Theoretical C_Q requirements for HLFC model as a function of chord Reynolds number with suction extending from $x/c = 0.025$ to 0.25. $M_\infty = 0.811$, $c_l = 0.483$.

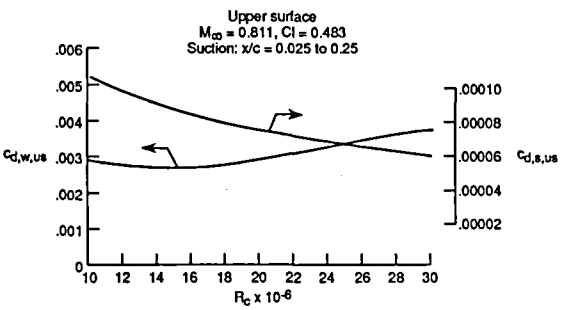

Figure 6. Wake-drag and equivalent-suction-drag predictions for the HLFC model as a function of chord Reynolds number. Suction extends from $x/c = 0.025$ to $x/c = 0.25$. $M_\infty = 0.811$, $c_l = 0.483$, and $\Lambda = 23°$.

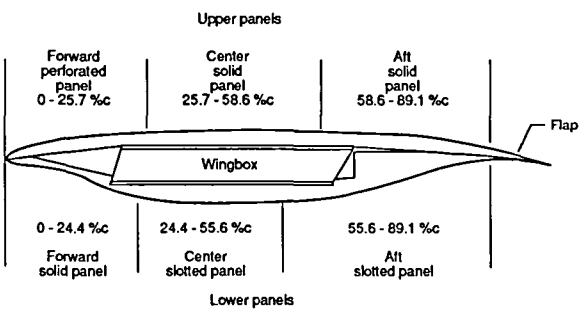

Figure 7. Location and chordwise extent of panels comprising surface of HLFC model.

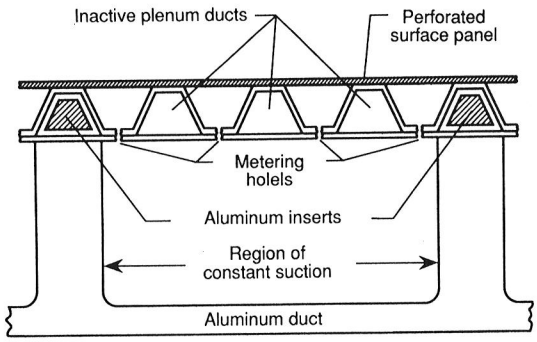

(a) Perforated panel construction features showing plenum ducts, metering holes and main duct.

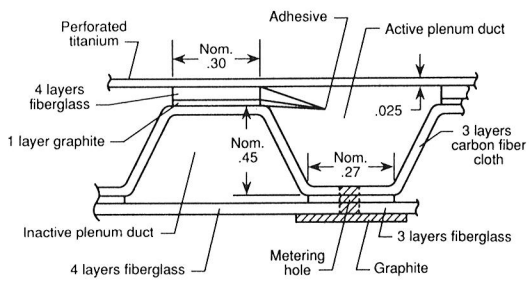

(b) Detail construction features of perforated surface showing materials used and nominal dimensions (in inches).

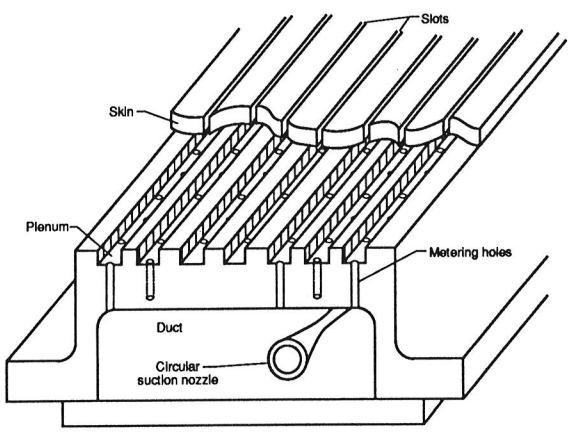

(c) Construction features of slotted panels showing slotted surface, slot plenums, metering holes, and main duct.

Figure 8. Construction features of perforated and slotted suction surfaces.

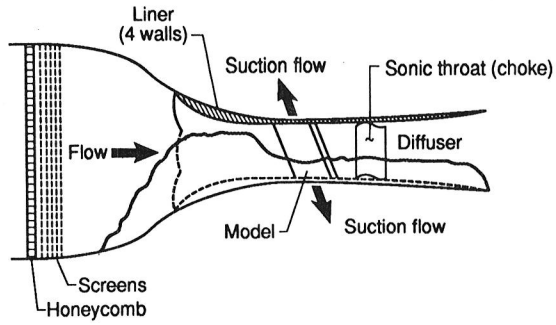

(a) Cross section of tunnel showing liner, model, and sonic choke.

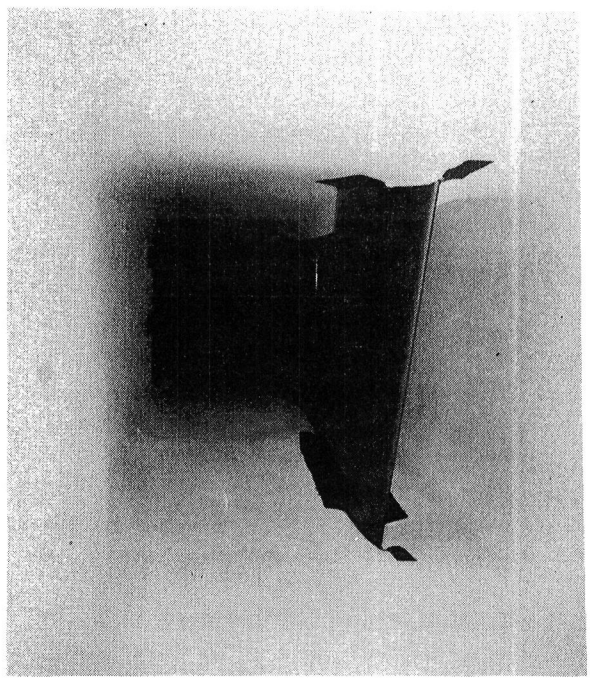

(b) Photograph of model installed in 8-ft TPT.

Figure 9. Sketch and photograph showing the special features of the test set up in the 8-ft TPT for LFC and HLFC testing.

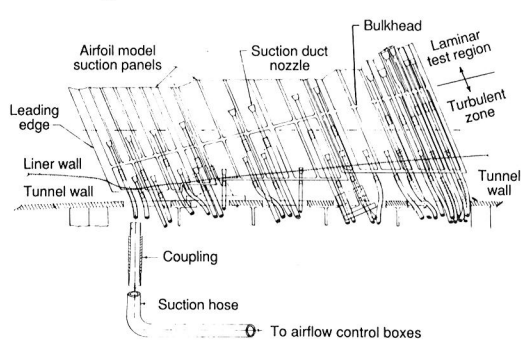

(a) Sketch of end of model nearest the test section floor showing the suction nozzles installed in the turbulent zone and laminar test regions.

Figure 10. Suction system for the HLFC and LFC experiments.

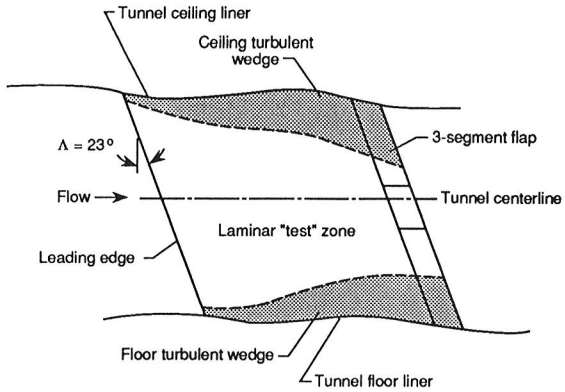

(b) Sketch of model showing geometry of the turbulent wedges or zones at the ends of the model as well as the laminar "test" zone.

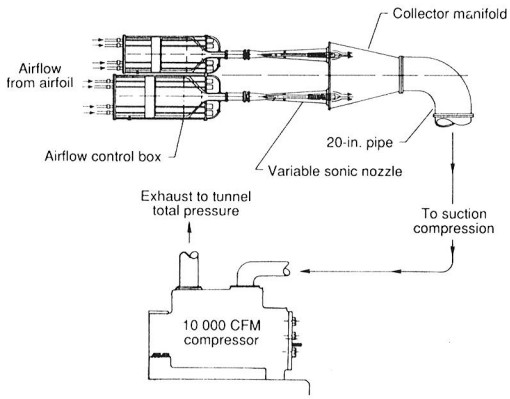

(c) Suction airflow system.

Figure 10. Concluded.

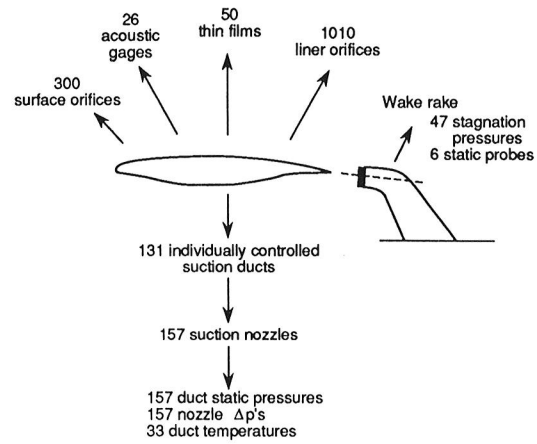

Figure 11. Sketch indicating type and number of sensors used in LFC and HLFC tests.

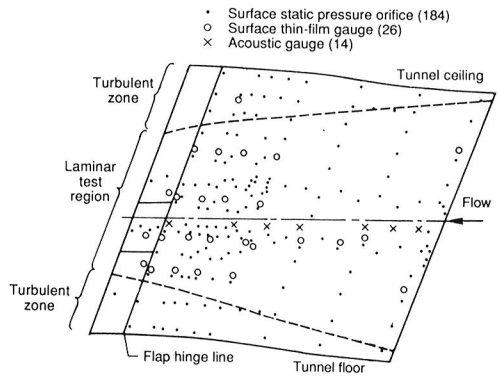

Figure 12. Sketch of LFC and HLFC model with location of pressure orifices, surface thin-film gauges and acoustic gauges. Upper surface.

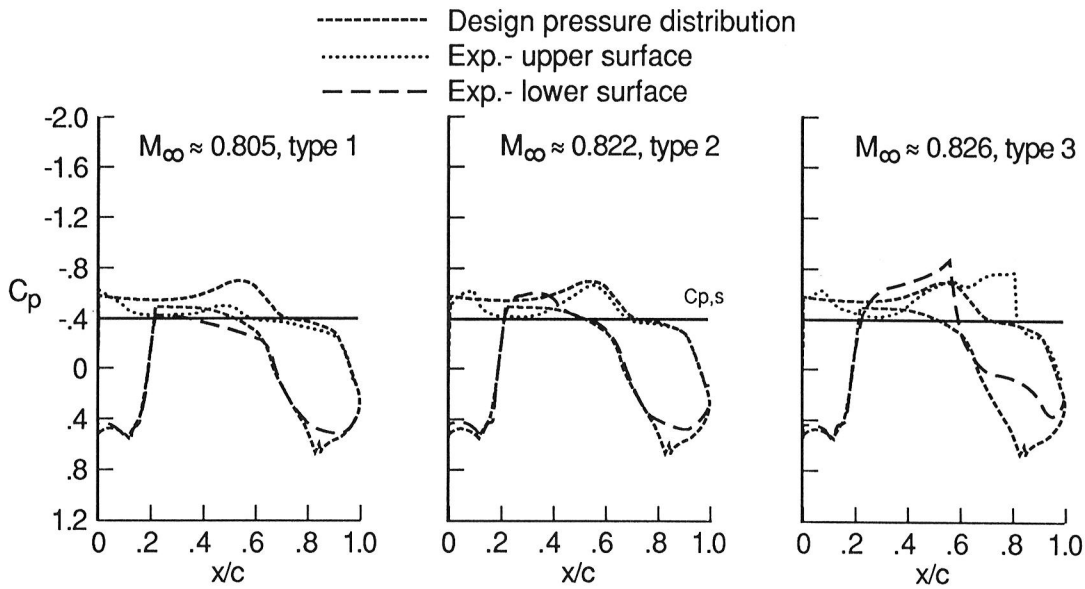

Figure 13. Three types of pressure distribution obtained on HLFC model. $R_c = 15 \times 10^6$, $\alpha = 0.028°$.

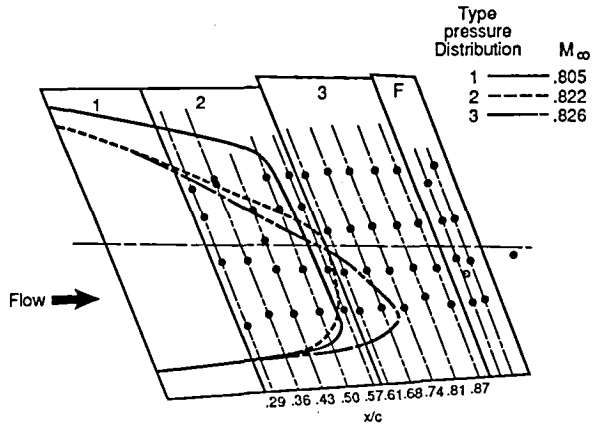

Figure 14. Transition boundaries for the three types of pressure distribution shown in Figure 31. $R_c = 15 \times 10^6$.

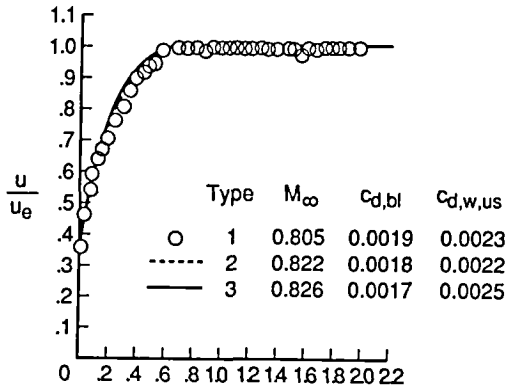

Figure 15. Boundary layer velocity distributions at the 95% chord location for the three types of pressure distribution shown in Figure 31. $R_c = 15 \times 10^6$.

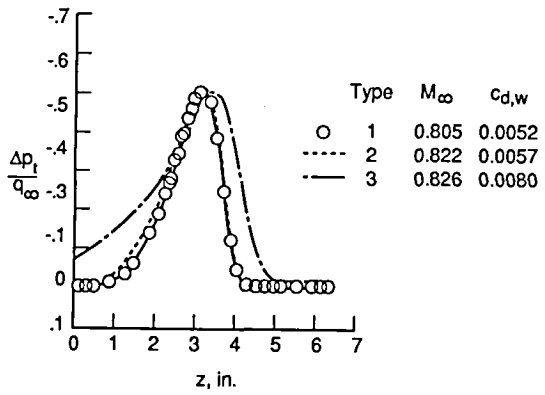

Figure 16. Wake total-head-defect profiles for the three types of pressure distribution shown in Figure 31. $R_c = 15 \times 10^6$.

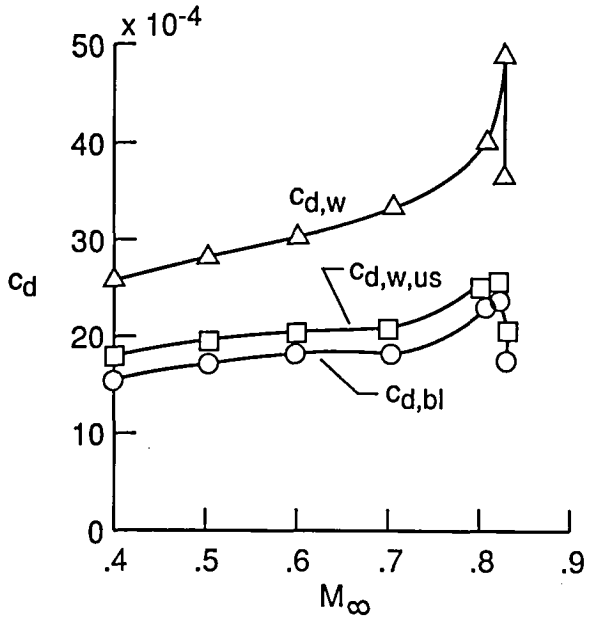

(a) Drag coefficients.

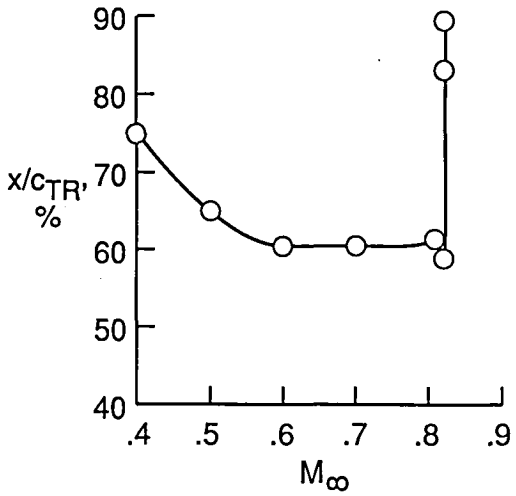

(b) Transition location.

Figure 17. Mach number variations of top-surface drag, airfoil wake drag, and transition locations for the HLFC model at $R_c = 10 \times 10^6$.

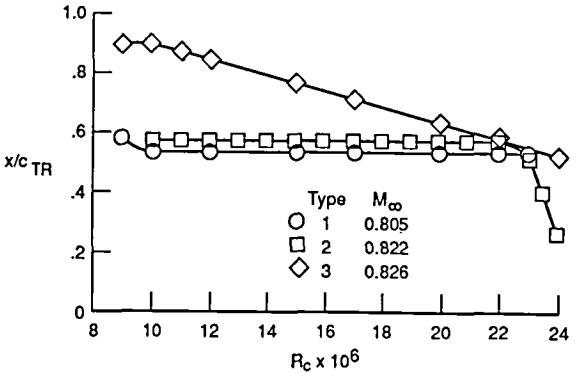

Figure 18. Variation of transition location with Reynolds number for the three types of pressure distribution shown in Figure 13.

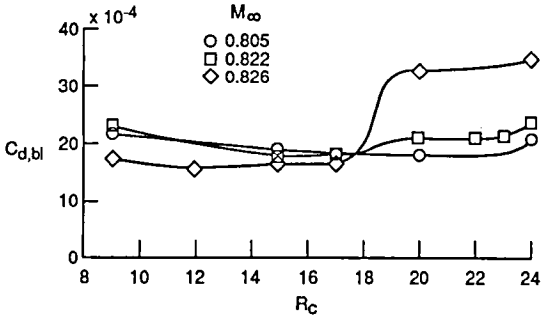

Figure 19. Variation of $c_{d,bl}$ with chord Reynolds number for the three types of pressure distribution.

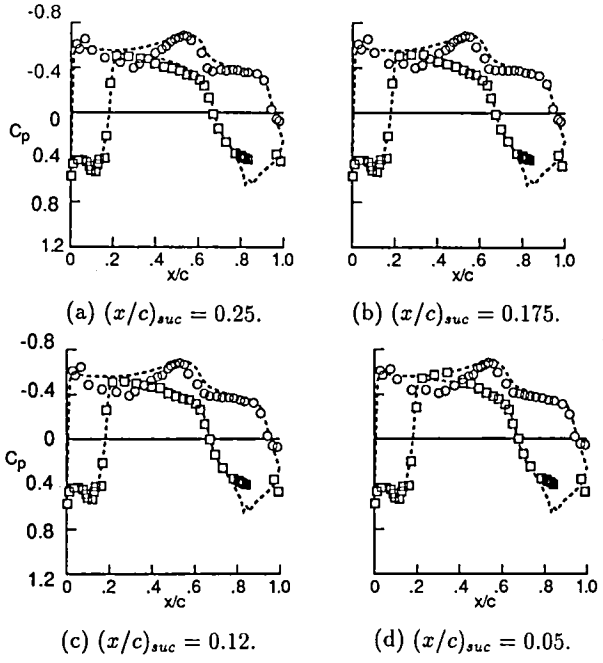

Figure 20. Type 2 pressure distributions for four chordwise extents of suction. $M_\infty = 0.82$, $R_c = 15 \times 10^6$.

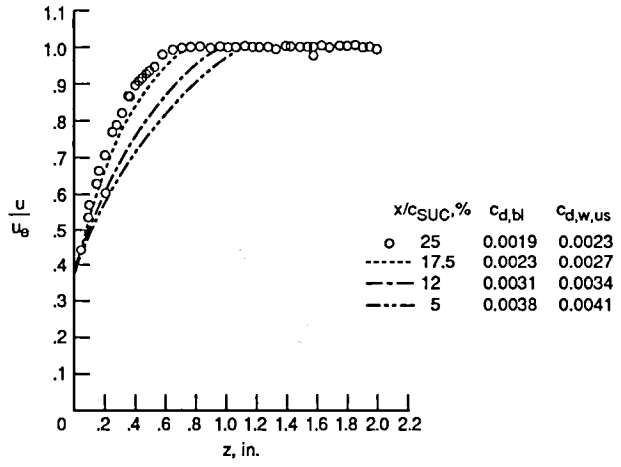

Figure 21. Boundary layer velocity profiles and top-surface drag coefficients for four chordwise extents of suction. $M_\infty = 0.82$, $R_c = 15 \times 10^6$.

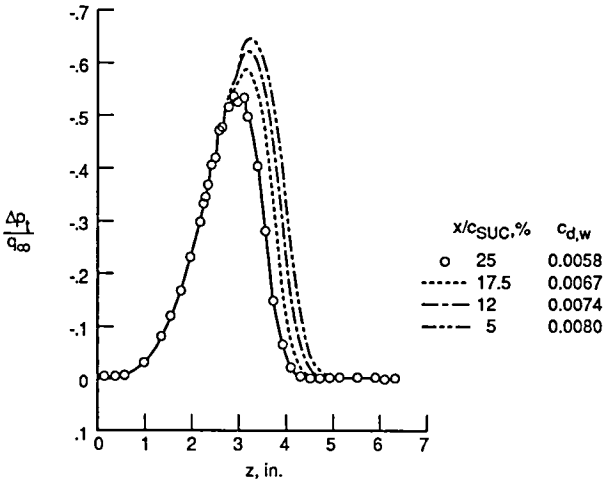

Figure 22. Total head-defect wake profiles and wake drag for four chordwise extents of suction. $M_\infty = 0.82$, $R_c = 15 \times 10^6$.

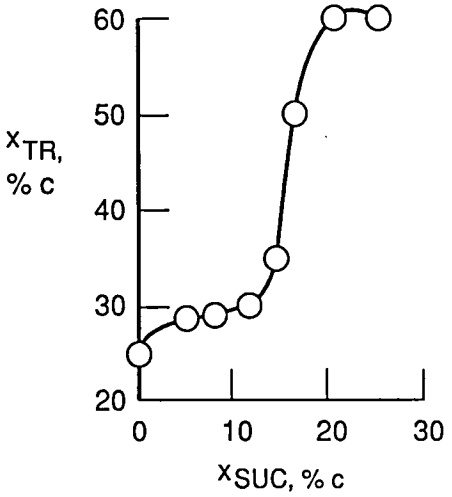

Figure 23. Transition location as a function of the chordwise extent of suction. $M_\infty = 0.82$, $R_c = 15 \times 10^6$.

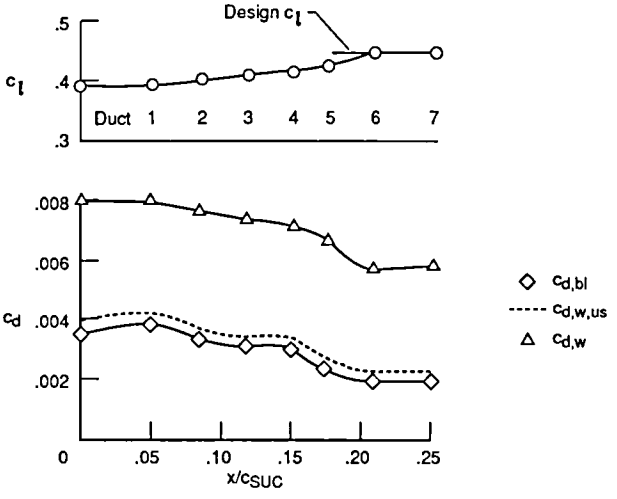

Figure 24. Top-surface and airfoil drag coefficients as a function of the chordwise extent of suction. $M_\infty = 0.82$, $R_c = 15 \times 10^6$.

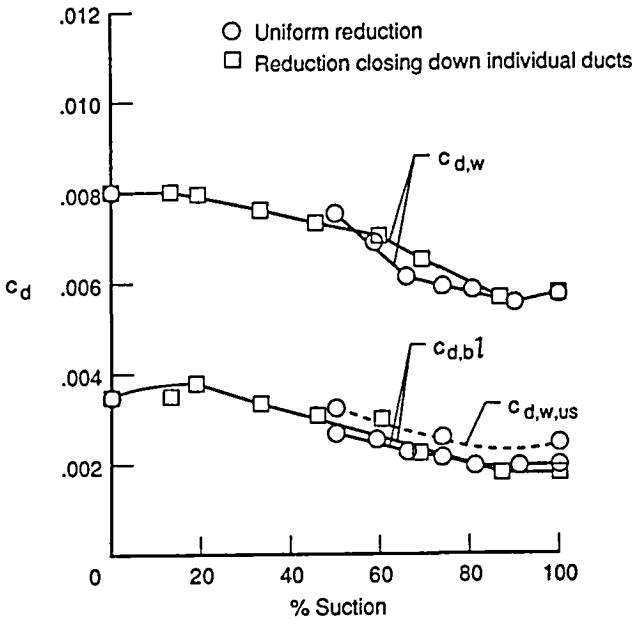

Figure 25. The variation of upper surface and airfoil drag coefficients with level of suction for two methods of reducing the suction level. $M_\infty = 0.82$, $R_c = 15 \times 10^6$.

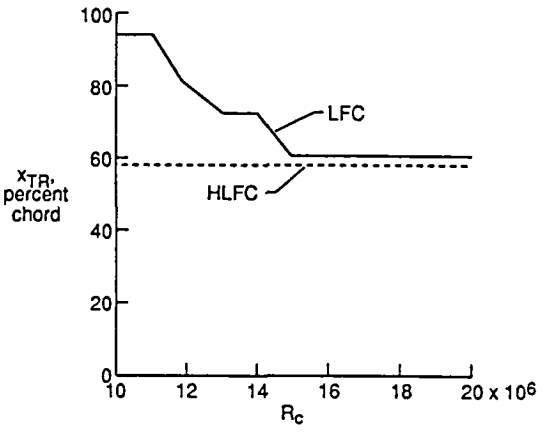

Figure 26. Transition location as a function of chord Reynolds number for the upper surfaces of the slotted LFC and HLFC models. $M_\infty = 0.82$.

REPORT DOCUMENTATION PAGE

Form Approved
OMB No. 0704-0188

1. AGENCY USE ONLY (Leave blank)	2. REPORT DATE	3. REPORT TYPE AND DATES COVERED
	March 1992	Technical Memorandum

4. TITLE AND SUBTITLE
Results for the Hybrid Laminar Flow Control Experiment Conducted in the NASA Langley 8-Ft Transonic Pressure Tunnel on a 7-Ft Chord Model

5. FUNDING NUMBERS
WU 505-69-20-01

6. AUTHOR(S)
Percy J. Bobbitt, James C. Ferris, William D. Harvey, and Suresh H. Goradia

7. PERFORMING ORGANIZATION NAME(S) AND ADDRESS(ES)
NASA Langley Research Center
Hampton, Virginia 23665-5225

8. PERFORMING ORGANIZATION REPORT NUMBER

9. SPONSORING/MONITORING AGENCY NAME(S) AND ADDRESS(ES)
National Aeronautics and Space Administration
Washington, DC 20546-0001

10. SPONSORING/MONITORING AGENCY REPORT NUMBER
NASA TM-107582

11. SUPPLEMENTARY NOTES
Bobbitt: Institute for Computer Applications in Science and Engineering, Hampton, VA; Ferris and Harvey: Langley Research Center, Hampton, VA; Goradia: Vigyan, Inc., Hampton, VA.

12a. DISTRIBUTION/AVAILABILITY STATEMENT
[redacted]
Subject Category 12

12b. DISTRIBUTION CODE

13. ABSTRACT *(Maximum 200 words)*

A description is given of the development of, and results from, the hybrid laminar flow control (HLFC) experiment conducted in the NASA Langley 8-foot Transonic Pressure Tunnel on a 7-foot chord, 23° swept model. The methods/codes used to obtain the contours of the HLFC model surface and to define the suction requirements are outlined followed by a discussion of the model construction, suction system, instrumentation and some example results from the wind tunnel tests. Included in the latter are the effects of Mach number, Reynolds number, suction level and the extent of suction. An assessment is also given of the effect of the wind tunnel environment on the suction requirements. The data show that, at or near the design Mach number ($M_\infty \approx 0.81$), large extents of laminar flow can be achieved with suction mass flows over the first 25%, or less, of the chord. Top surface drag coefficients with suction extending from near the leading edge to 20% of the chord were approximately 40% lower than those obtained with no suction. The results indicate that HLFC an be designed for transonic speeds with lift and drag coefficients approaching those of LFC designs but with much smaller extents and levels of suction.

14. SUBJECT TERMS		15. NUMBER OF PAGES
Laminar Flow Control Swept, Supercritical Airfoil Suction	Perforated Suction Surface Transonic Wind Tunnel Tests	17 16. PRICE CODE

17. SECURITY CLASSIFICATION OF REPORT	18. SECURITY CLASSIFICATION OF THIS PAGE	19. SECURITY CLASSIFICATION OF ABSTRACT	20. LIMITATION OF ABSTRACT
UNCLASSIFIED	UNCLASSIFIED	UNCLASSIFIED	

DO NOT REMOVE SLIP FROM MATERIAL

Delete your name from this slip when returning material to the library.

NAME	DATE	MS

NASA Langley (Rev. Dec. 1991) RIAD N-75